AUT Journal of Mechanical Engineering

AUT J. Mech. Eng., 5(4) (2021) 553-570
DOI: 10.22060/ajme.2021.18838.5924

Out of Plane Punch of Aluminum Hexagonal Honeycomb Using Flat Nose and Spherical Projectiles

M. Zarei Mahmoudabadi, M. Sadighi*

Department of Mechanical Engineering, Amirkabir University of Technology, Tehran, Iran

ABSTRACT: The energy absorption capacity of metal hexagonal honeycomb under out of plane local quasi-static loading is investigated, experimentally. Effects of geometrical parameters, such as the cell size and wall thickness of the honeycomb, projectile shape and projectile diameter, specimen height, and the loading speed on the perforated zone and the absorbed energy are studied. The perforated zone of the honeycomb has not perfectly the same shape of the projectile, but it can be assumed as a skew polygon or ellipse, extended in the direction of the honeycomb dual walls. Results show that changing the projectile shape from a flat nose to a sphere decreases the absorbed energy approximately to the half value. Multiplying the projectile diameter by two increases the mean crushing load of the metal hexagonal honeycomb less than four times. On the other hand, it was shown that the honeycomb local energy absorption capacity is not perfectly independent of sample height and loading speed. Furthermore, based on the modified Wierzbicki's model in the global loading, a simple theoretical model for the estimation of the mean crushing load of a metal hexagonal honeycomb loaded by a flat projectile is presented. Good agreement between the theoretical and experimental results is illustrated.

Review History:

Received: Aug. 06, 2020
Revised: Dec, 11, 2020
Accepted: Jan. 22, 2021
Available Online: Mar. 05,2021

Keywords:

Metal hexagonal honeycomb
local loading
Perforated zone
Theoretical model

1- Introduction

Honeycomb cellular structures, due to their light weights and high energy absorbing capability, have been used extensively as energy absorbers or cushions to resist external loads. Static and dynamic experimental tests, performed by Goldsmith and Sackman, showed that the dynamic crushing strength of the aluminum honeycomb is between 30% to 50% greater than its static one [1]. Wu and Jiang [2] investigated the geometrical parameters on the energy absorption capacity of aluminum honeycomb and found the important role of the cell size; although, their calculations must be modified [3]. Klintworth and Stronge [4] studied the behavior of the metallic honeycomb to in-plane quasi-static flat projectile loading. Galehdari et al. [5] investigated quasi-static and low velocity impact in-plane loading on the metal hexagonal honeycombs, experimentally, numerically, and analytically. They showed that the in-plane plateau stress of the honeycomb can be modeled as the "V" deformation mode. Goldsmith and Louie [6] performed an experimental investigation on the effects of cell size and wall thickness on the honeycomb's penetration limit. Their results showed that both increasing the cell size and decreasing the wall thickness decrease the absorbed energy. Effect of the geometrical parameters and the degree of constraint associated with the bonding of the honeycomb to face-sheet on the out-of-plane compressive response of stainless steel square honeycombs studied by Cote et al. [7]. Heimbs et al. [8] showed that the strain rate has a nonlinear effect on the honeycomb strength and in the low velocity impact loading can be ignored. Alavi Nia et al. [9] determined the ballistic limit of aluminum honeycomb with the different cell size and wall thickness, experimentally. Asada et al. [10] studied the in-plane flat punch indentation of the honeycomb, experimentally and numerically. Khoshravan and Najafi Pour [11] using homogeneous and non-homogeneous finite element methods, illustrated that the energy absorption capacity of aluminum honeycomb increases with decreasing cell size and increasing cell wall thickness. Weia et al. [12] illustrated that the metallic honeycomb strength under global loading is more than the strength of a metal plate with the same weight, while in the local loading the metal plate strength is more. Low velocity impact tests on polymeric honeycombs performed by Petrone et al. [13] showed that the being or not being the facesheet is not significant for the high thickness specimens. Partovi meran et al. [14] studied the behavior of metal hexagonal honeycomb under out of plane global impact loading, numerically and showed that crashworthiness parameters depend on cell specification and wall thickness of the honeycomb structure and are independent of impact mass and velocity. Zarei Mahmoudabadi and Sadighi [15] investigated the energy absorption characteristics of sandwich panels with an aluminum plate as facesheet and metal hexagonal honeycomb as the core under quasi-static

*Corresponding author's email: mojtaba@aut.ac.ir

Table 1. specifications of honeycomb specimens

Sample Index	Cell Size (mm)	Wall Thickness (mm)	Specimen's Height (mm)	Projectile Shape	Projectile Diameter (mm)	Loading Speed (mm/min)
SM1	3.29	0.0254	20.0	Global	-	2
SM2	7.00	0.0508	18.0	Global	-	2
SM3	3.29	0.0254	20.0	Flat	32	2
SM4	3.29	0.0254	20.0	Flat	16	2
SM5	7.00	0.0508	18.0	Flat	32	2
SM6	7.00	0.0508	18.0	Flat	16	2
SM7	3.29	0.0254	20.0	Sphere	16	2
SM8	7.00	0.0508	18.0	Sphere	16	2
SM9	3.29	0.0254	12.7	Flat	16	2
SM10	3.29	0.0254	12.7	Sphere	16	2
SM11	3.29	0.0254	20.0	Flat	16	100
SM12	3.29	0.0254	20.0	Sphere	16	100

punch loading using two flat nose and spherical projectiles, experimentally. They classified the failure modes as plastic hinges, facesheet wrinkling, debonding of the adhesive layer between the facesheet and core, facesheet tearing, out of plane core crushing, in-plane core folding, core tearing and detachment from the support. Wang et al. [16] expanded the honeycomb structure panel to cylindrical shell by adopting the rolled-up algorithm and discussed on the crushing behaviors of the Randomly Honeycomb Cylindrical Shell (RHCS) structures under axial loading. They found that the deformation modes of RHCS structures are significantly affected by thickness-to-diameter ratio and cell irregularity.

Wierzbicki [17] presented a theoretical model for the prediction of mean crushing load and half-wavelength of folding mode in the honeycomb out of plane quasi-static global loading.

Abramowicz and Wierzbicki [18] illustrated that abnegation of stretching mode and only considering the not stretching mode for determination of the honeycomb strength has not significantly error. Zarei Mahmoudabadi and Sadighi [19] modified Wierzbicki's model by considering the curvature effect and flow stress and improved it to study the behavior of metallic honeycomb under low velocity impact loading [20]. The plastic collapse stress under in-plane static compression was investigated mathematically and numerically by Zhen et al. [21] results show that the plastic collapse stress in the *y*-direction is larger than that in the *x*-direction under multi-cell conditions. However, it turns to be insignificant when the crushing velocity reaches or exceeds a critical velocity. They extended their theoretical model in the estimation of the mean crushing load of the foam filled metal hexagonal honeycomb and compared their theory with the experimental data [22].

It can be seen that most articles in the literature have studied the global crushing behavior of metallic honeycombs. On the other hand, Identifying the failure modes and energy absorption characteristics of hexagonal honeycomb under local punch loading is a very important step in the perforation and penetration analyses of sandwich panels with honeycomb core under out of plane loading by the projectile. In this article, the crushing behavior of aluminum hexagonal honeycomb under local quasi-static loading has been studied, experimentally. Investigated parameters are honeycomb cell size, wall thickness, specimen height, projectile shape, projectile diameter, and loading speed. In addition, a theoretical model has been developed to estimate the behavior of these energy absorbers loaded by flat nose projectiles. This theoretical model can be extended to study the behavior of the honeycomb core sandwich structures in the future.

2- Experiment

The local quasi-static tests have been performed on aluminum hexagonal honeycomb specimens using the universal testing machine. Variable parameters are the cell size and the wall thickness of the honeycomb, projectile nose, projectile diameter, specimen height, and loading speed. Table 1 describes the specifications of each test. Three specimens used for each tested condition and the average value of them reported ensuring the reliability of tested data. In order to determine the contribution of each absorbed energy terms, the global out of plane pressure has been carried out on specimens 1 and 2. Samples are placed on a rigid flat plate to achieve the fully backed conditions (Fig. 1).

Concertina mode folding has been seen in all of the specimens. Fig. 2 shows specimens SM1 and SM2 before global compressive loading and after it.

Load-displacement curves of samples SM1, SM3, SM5, SM7, and samples SM2, SM5, SM6, and SM8 have been shown in Figs. 3 and 4, respectively. In order to determine the dissipated energy terms in local loading, the load-displacement diagrams of samples SM1 and SM2 have been scaled for a circular sample with a diameter of 32 mm.

Fig. 1. Testing conditions of a sample under flat projectile.

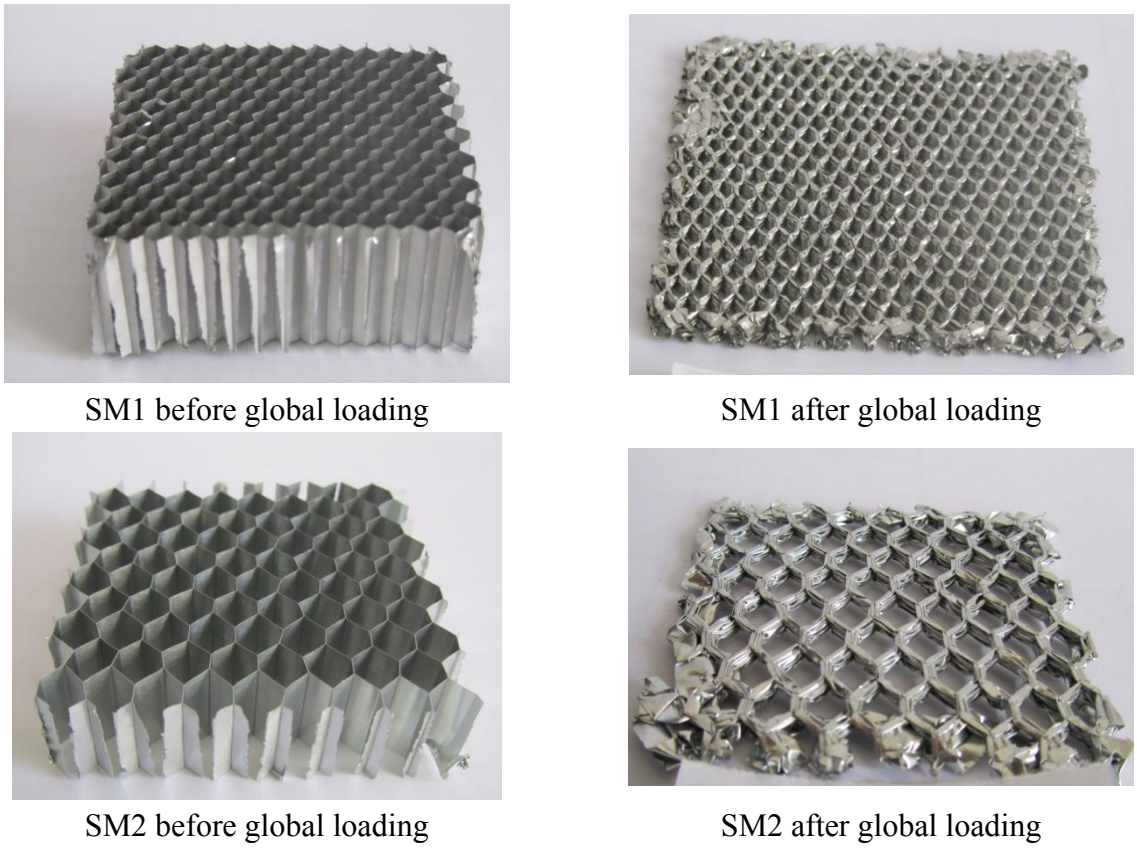

Fig. 2. Samples SM1 and SM2 before global compressive loading and after it.

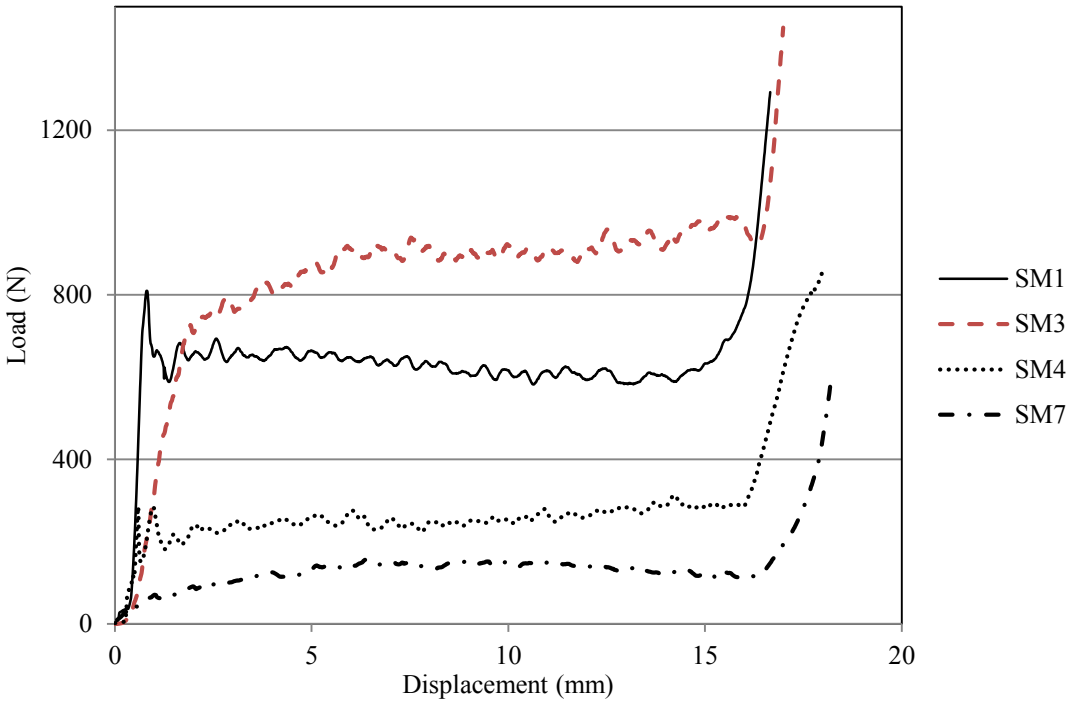

Fig. 3. Load-displacement curves of samples SM1, SM3, SM4, and SM7.

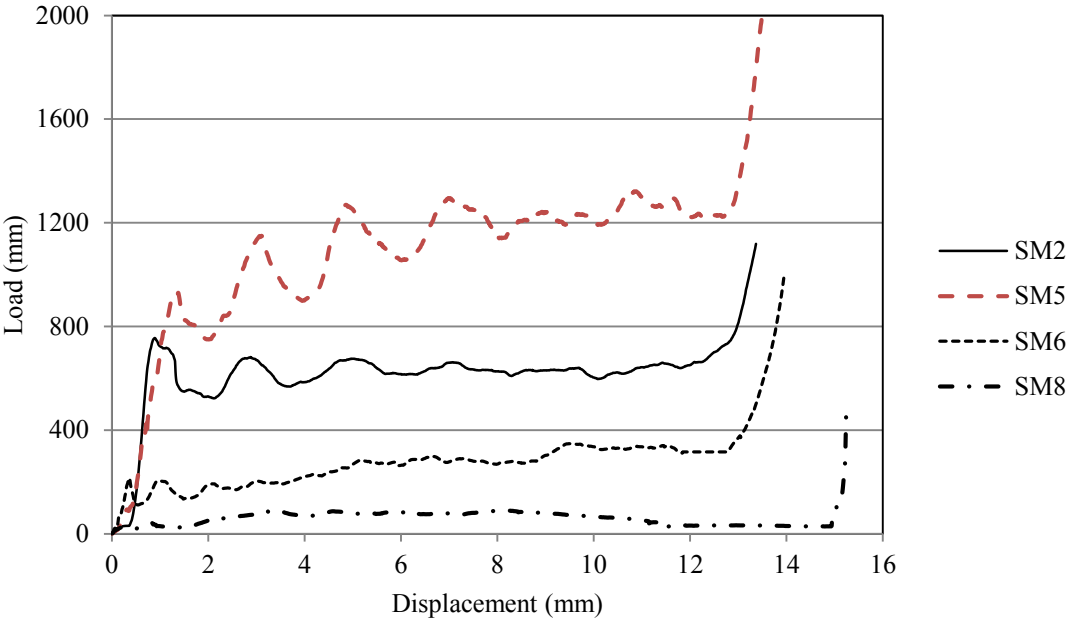

Fig. 4. Load-displacement curves of samples SM2, SM5, SM6, and SM8.

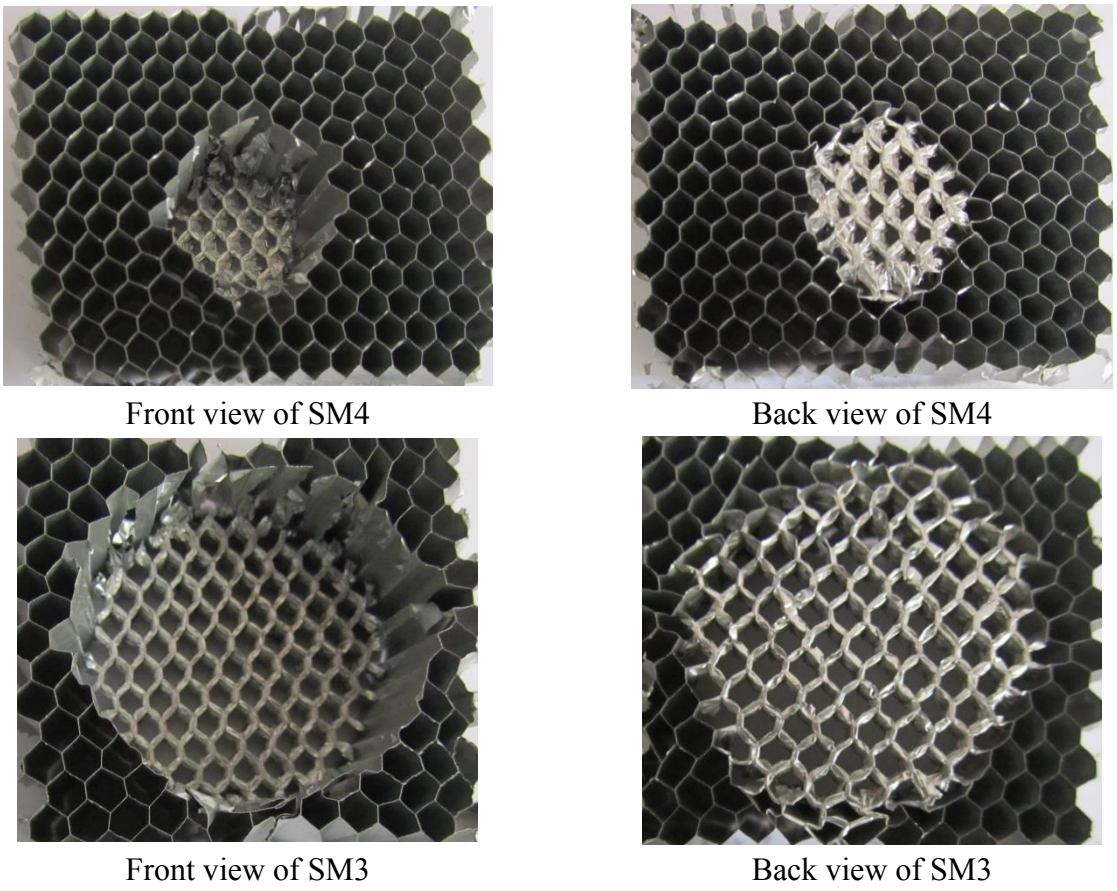

Fig. 5. Front and back views of SM3 and SM4.

2- 1- Flat projectile loading

The front and back views of samples SM3, SM4, and samples SM5, SM6 have been shown in Figs. 5 and 6, respectively. It can be seen that the perforated zones of the honeycomb samples are not perfectly circular, but they are similar to skew polygons. However, the perforated zone is led to a circle by increasing the projectile diameter. Polygon has been extended in direction of the dual walls when the major diameter of the polygon is in the dual wall direction, but its minor diameter is perpendicular to the dual walls. On the other hand, increasing the cell size leads to the in-plane distortion of the cells that are established in the polygon major diameter direction more than the other cells (See Fig. 6).

Figs. 3 and 4 show that the load-displacement diagram of a metal hexagonal honeycomb under local flat projectile loading is typically the same as its global loading, Although, the peak load does not appear at the end of the elastic zone, the plateau section of the curve is ascendant, and the mean crushing force is significantly greater than that of the global loading. A shear energy term, required for the perforation of the flat projectile into the honeycomb and cutting off the cells, increases the total dissipated energy. On the other hand, the polygon area is greater than its surrounded circle, therefore the crushing energy term increases. Finally, a small energy term, dissipated in the in-plane distortion of the cells, can be added to the internal dissipated energy.

Comparison between SM3 and SM4, and between SM5 and SM6 illustrates that multiplying the cross-sectional area of the flat projectile by four increases the mean crushing load of the aluminum honeycomb less than four times. The shear energy term is related to the projectile ambient and so related linearly to the projectile diameter. On the other hand, increasing the projectile diameter results that the skew polygon leads to a circle with a radius nearly equal to the projectile radius.

2- 2- Spherical projectile loading

The load-displacement diagram of the aluminum honeycomb loaded by a spherical projectile is different from that of the flat projectile (see Figs. 3 and 4). The force

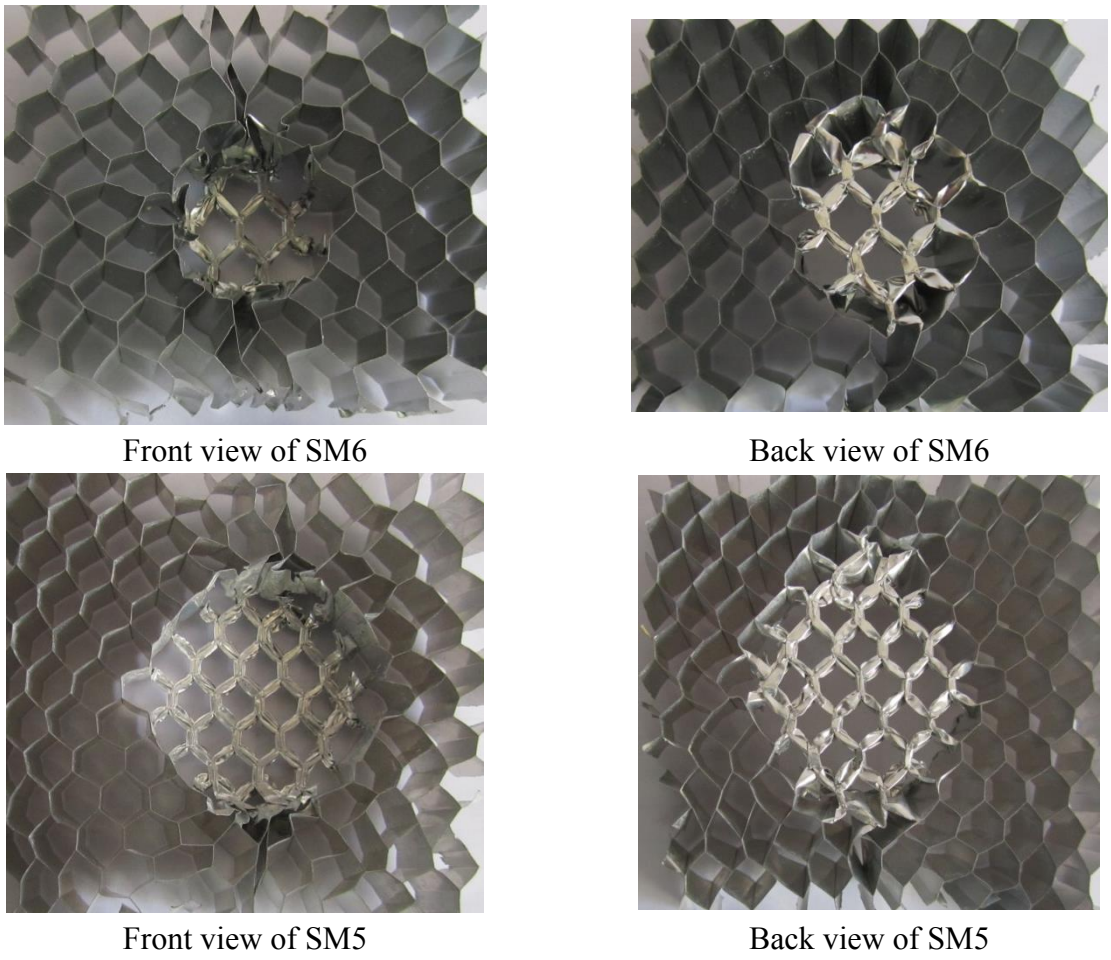

Fig. 6. Front and back views of SM5 and SM6.

increases continuously to a maximum value, corresponding to a displacement approximately equal to the projectile radius. Increasing the area of the contact zone before that force reaches the maximum value causes to increase in the dissipated energy. On the other hand, after the maximum point, the load decreases smoothly which can be described by attention to Fig. 7. Spherical projectile squeezes the honeycomb walls near to the projectile ambient in the in-plane direction. Since the in-plane honeycomb stiffness is significantly less than that of the out-plane one, the load decreases smoothly. In-plane pressure causes the maximum load of a honeycomb under spherical projectile loading to be about only half of the maximum load in the flat projectile loading. Fig. 7 shows that the perforated zone of the honeycomb loaded by a spherical projectile is similar to an elliptical shape, extended in the dual walls direction.

2- 3- Effect of sample height

Fig. 8 shows the load-displacement diagrams of samples SM9, and SM10. For better comparison, the load-displacement curves of samples SM4, and SM7 are plotted again. It can be seen that the behavior of aluminum hexagonal honeycomb is not perfectly independent of sample height, but increasing the height decreases slightly the mean crushing load of honeycomb. When the displacement in sample SM10 is near to 6 mm (slightly less than the indenter radius) the force reaches its maximum value in this case because the sample height is not properly adequate. On the other hand, in this sample, the load decreases strongly after the peak value that can be the reason for the cutting-off of the honeycomb panel.

The front and back views of samples SM9 and SM10 are shown in Fig. 9. It can be seen that the skew polygon and elliptical shape, both are extended in the dual walls direction, are appeared. However, they are not obvious as those of samples SM4 and SM7.

2- 4- Effect of loading speed

Effect of loading speed on the behavior of the metal hexagonal honeycomb under local loading can be illustrated

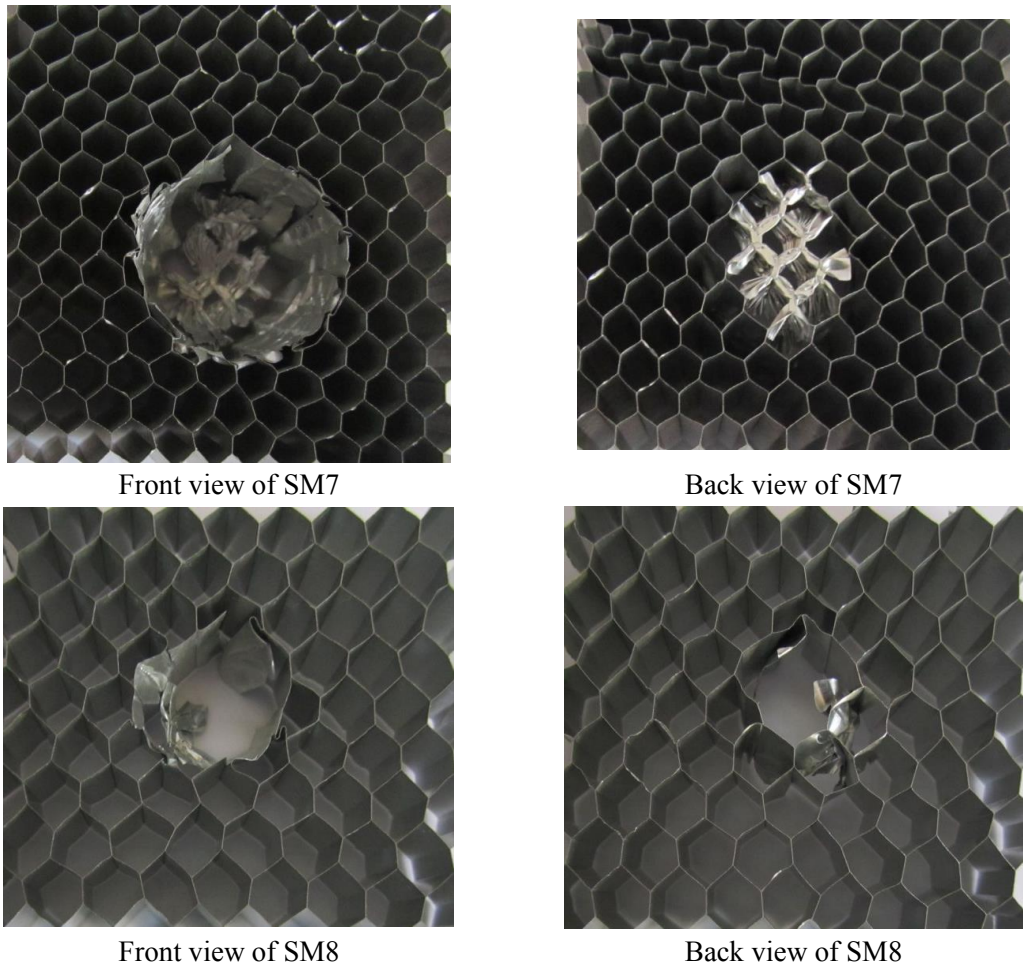

Fig. 7. Front and back views of SM7 and SM8.

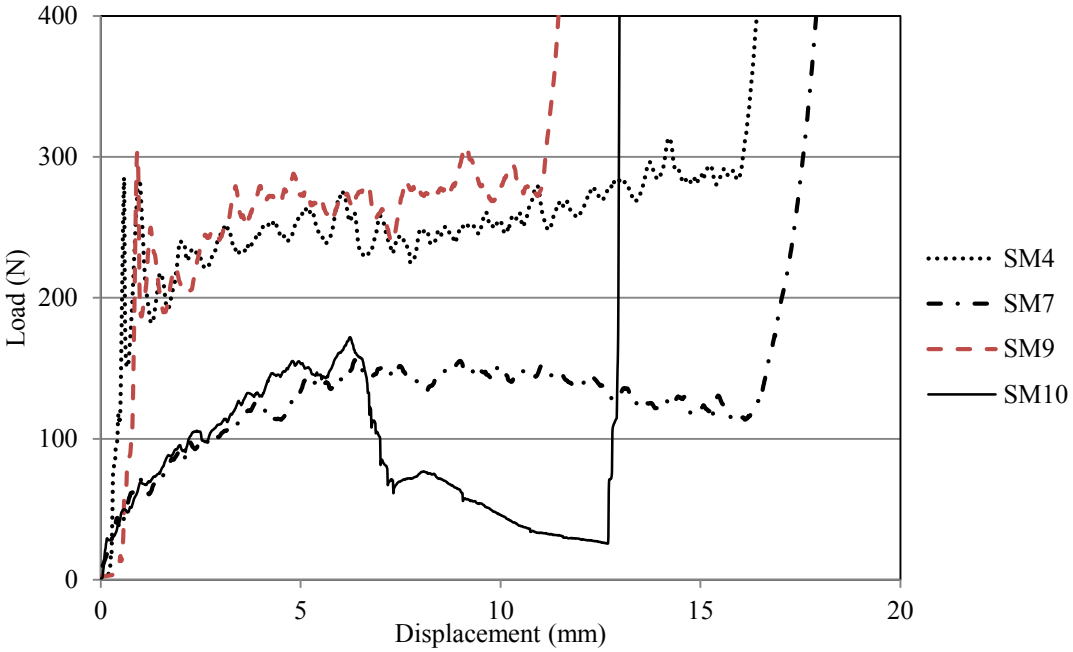

Fig. 8. Load-displacement diagrams of samples SM4, SM7, SM9, and SM10.

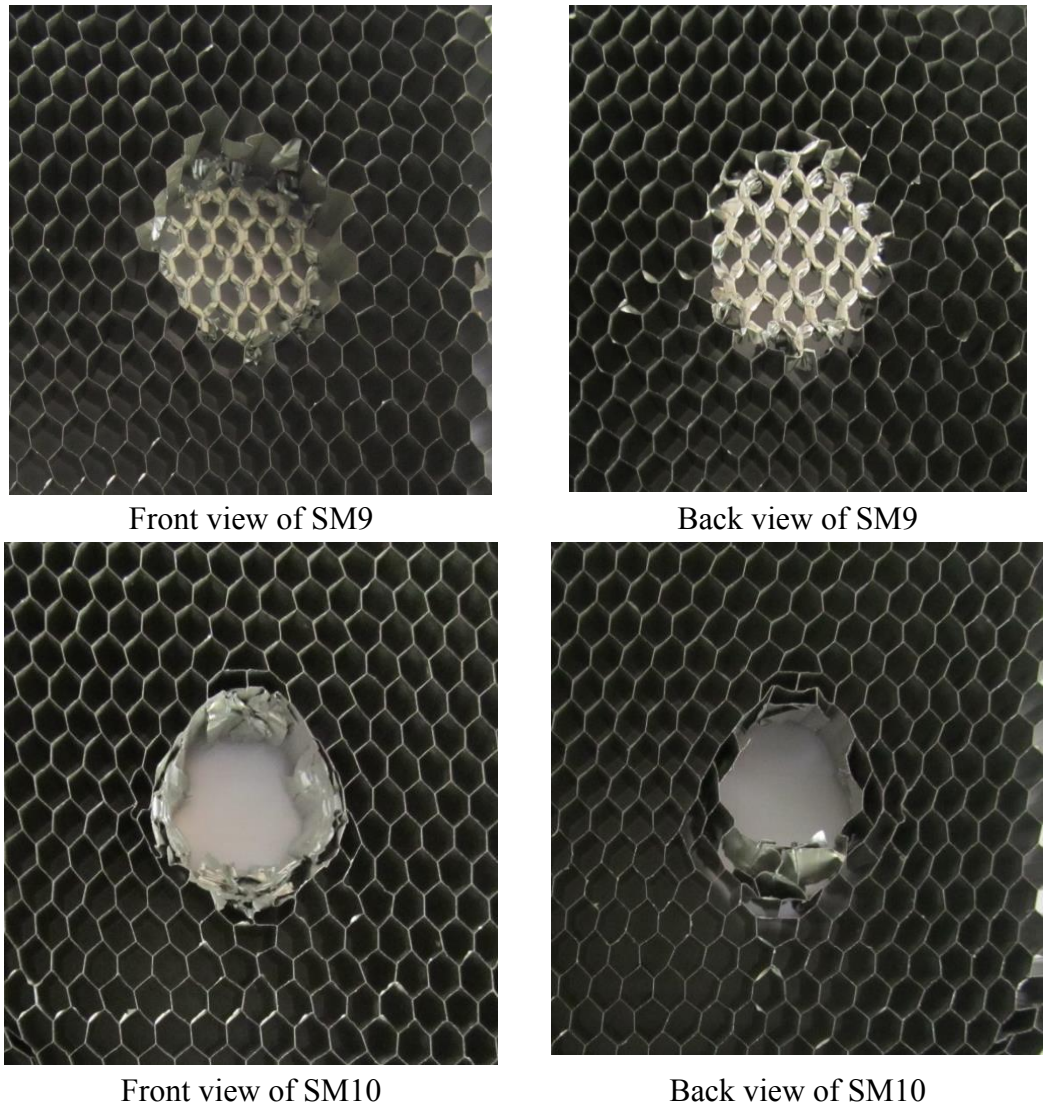

Fig. 9. Front and back views of SM9 and SM10.

from comparison samples SM11 and SM12 with SM4 and SM7. Fig. 10 shows that the effects of loading speed on the flat projectile loading are meaningless, while its effect on the load-displacement curve of the honeycomb under spherical indenter is more. Increasing the loading speed leads to cutting-off the honeycomb panel and decreasing the load value after the maximum point, although the maximum load value is approximately constant.

The difference between the perforated zone and projectile cross-section increases by increasing the loading speed, as the polygon changes to a rhombic shape and the difference between the major and minor diameters of ellipse increases (Fig. 11).

3- Analytical Model

In this section, a semi-analytical model for determining the mean crushing load of metal hexagonal honeycomb under quasi-static local loading, by a flat projectile, is presented using the energy method.

Internal dissipated energy of the metal honeycomb under local loading can be determined as Eq. (1), in which $E_{Crushing}$ and $E_{shearing}$ are the dissipated energy terms in out of plane crushing and cutting off of the honeycomb walls, respectively.

$$E_{\text{int}} = E_{Crushing} + E_{Shearing} \tag{1}$$

Considering a basic folding element shown in Fig. 12, $E_{Crushing}$ can be calculated as Eq. (2), where n_A is the

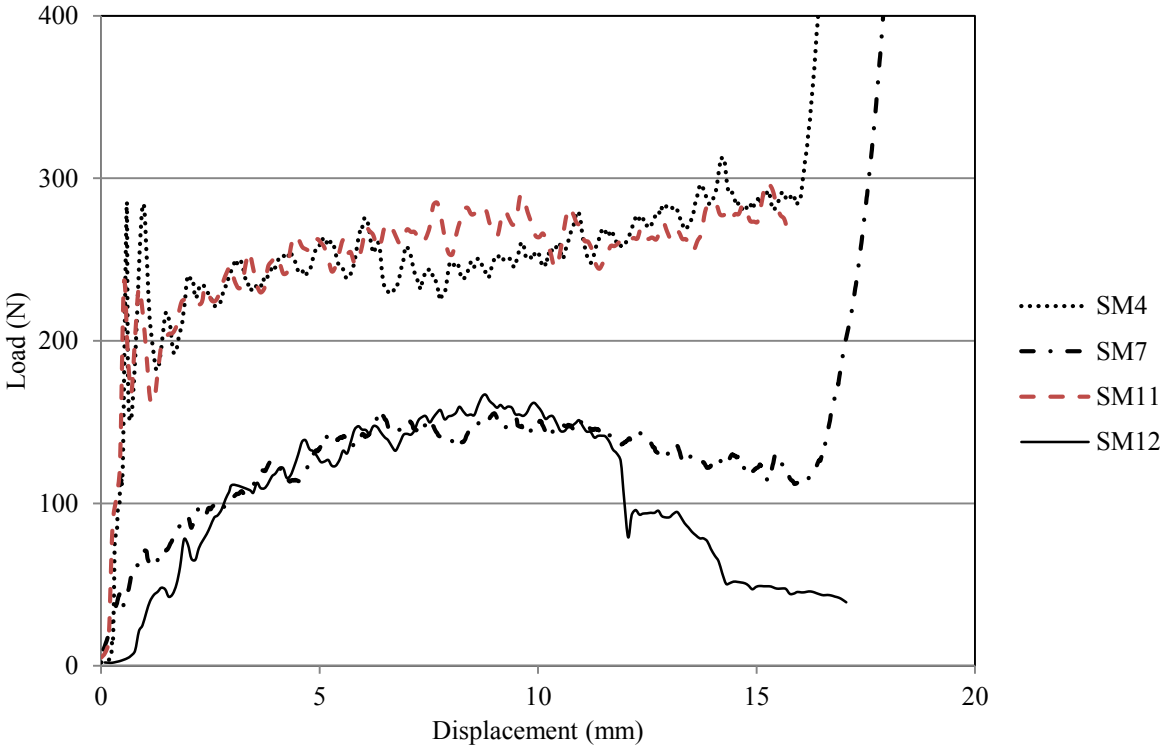

Fig. 10. Load-displacement diagrams of samples SM4, SM7, SM9, and SM10.

number of crushed folding elements and $e_{Basice\,element}$ is the dissipated energy due to crushing of a folding element:

$$E_{\text{int}} = n_A e_{Basice\,element} \tag{2}$$

Dissipated energy due to the crushing of a folding element, $e_{Basice\,element}$, has been calculated in Ref. [20] as:

$$e_{Basice\,element} = E_1 + E_2 + E_3 \tag{3}$$

Where

$$E_1 = 32M_0 \frac{Hb}{h} I_1(\psi_0) \tag{4-a}$$

$$E_2 = 4\sqrt{3}M_0 S\bar{\alpha} \tag{4-b}$$

$$E_3 = 8M_0 \frac{H^2}{b} I_3(\psi_0) \tag{4-c}$$

in which S and h are the cell size and the thickness of the cell wall, H is the half-wavelength of the folding mode, b is the small radius of the toroidal shell, and M_0 denotes the fully plastic bending moment and can be determined as:

$$M_0 = \frac{1}{4}\sigma_0 h^2 \tag{5}$$

where σ_0 is the flow stress of the honeycomb material. Furthermore, $I_1(\psi_0)$ and $I_3(\psi_0)$ can be determined as follow:

$$I_1(\psi_0) = \frac{3\sqrt{3}}{4}\int_0^{\bar{\beta}} \frac{1+\tan^2\beta}{(1+\sin^2\psi_0\tan^2\beta)^{3/2}} \times \tag{6-a}$$

$$\left[\cos\psi_0 - \cos\left(\psi_0 + \tfrac{2}{3}\beta\right)\right] d\beta$$

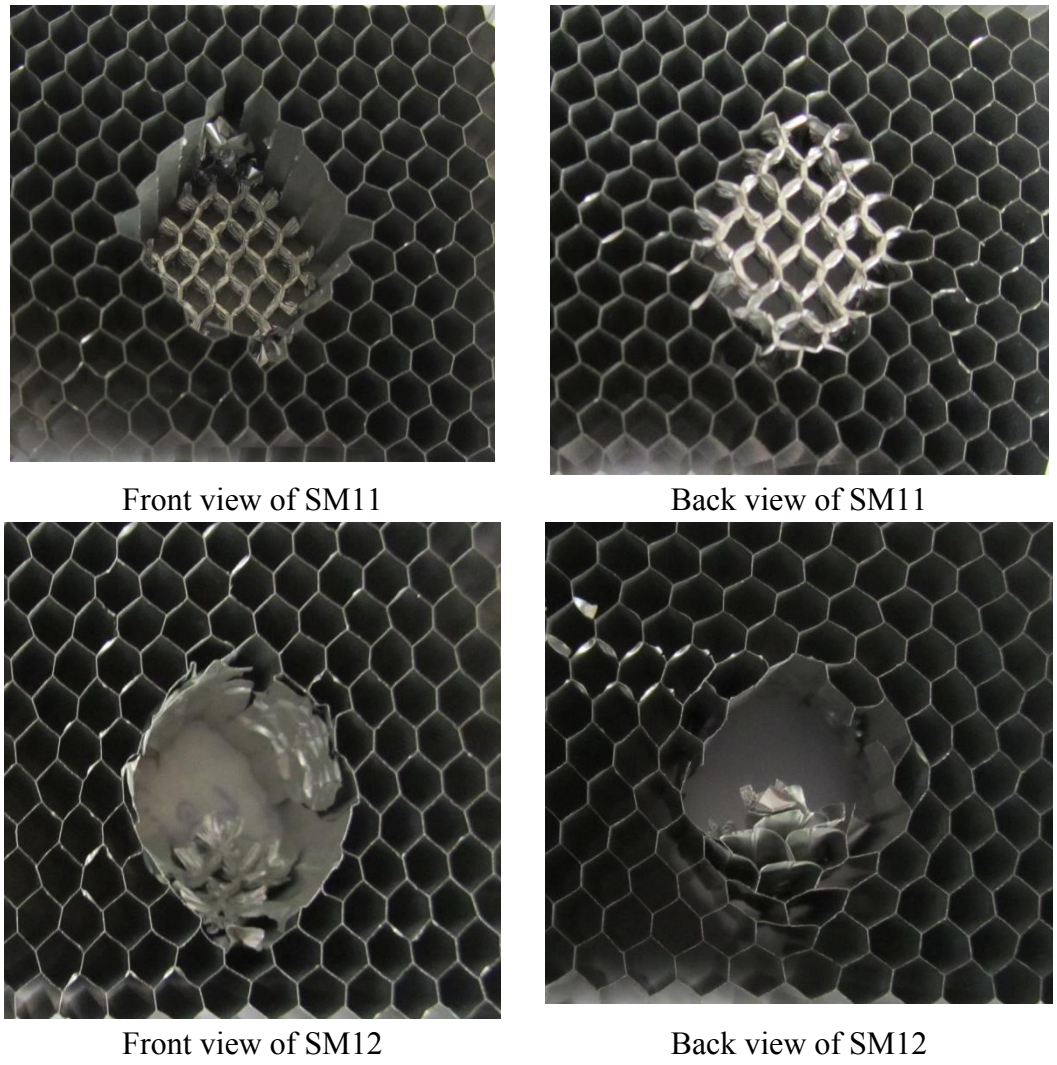

Fig. 11. Front and back views of SM11 and SM12.

$$I_3(\psi_0)=\left[\frac{\sin x}{2\cos^2 x}+\frac{1}{2}\ln\left(\tan\left(\frac{\pi}{4}+\frac{x}{2}\right)\right)\right]_0^{x_2} \quad (6\text{-b})$$

in which

$$\bar{\beta}=\tan^{-1}\left(\frac{\tan\bar{\alpha}}{\sin\psi_0}\right) \quad (7\text{-a})$$

$$x_2=\tan^{-1}\left(\frac{\sin\bar{\alpha}}{\tan\psi_0}\right) \quad (7\text{-b})$$

For a hexagonal honeycomb, $\psi_0=\pi/6$. In addition:

$$\bar{\alpha}=\frac{2H/b+\pi-\sqrt{(2H/b-\pi)^2-8}}{4} \quad (8)$$

Dissipated energy term in cutting-off of the honeycomb walls, $E_{shearing}$, is written as:

$$E_{Shearing}=n_w A_w E_s \quad (9)$$

in which E_s is the fracture energy per unit area of honeycomb materials, n_w is the number of the sheared walls, and A_w is the cross-sectional area of a honeycomb wall that can be written as:

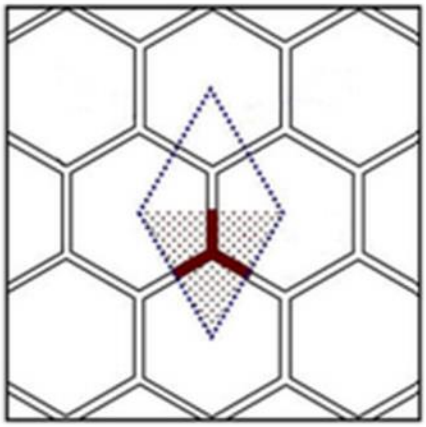

Fig. 12. A basic folding element

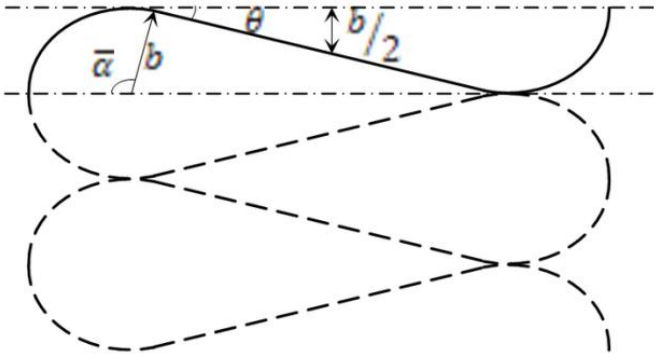

Fig. 13. Schematic lateral view of a honeycomb cell wall's final position [20].

$$A_w = 2hH \tag{10}$$

Substituting the crushing and shearing energy terms from Eqs. (2) and (9) into Eq. (1) and implementing Eq. (3) gives the internal dissipated energy of the metal hexagonal honeycomb under local quasi-static loading:

$$E_{\text{int}} = n_A \left(E_1 + E_2 + E_3\right) + n_w A_w E_s \tag{11}$$

A schematic lateral view of a honeycomb cell wall's final position, folded through local loading, has been presented in Fig. 13. Effective crushing distance, through which the mean crushing force, P, acts is $(2H - b)$ and the external work done by the projectile can be determined as:

$$E_{ext} = P(2H - b) \tag{12}$$

Equalization of the internal energy and the external work and using Eqs. (4) and (10) results in:

$$P(2H - b) = n_A M_0 \times \left[32\frac{Hb}{h} I_1(\psi_0) + 4\sqrt{3}S\bar{\alpha} + 8\frac{H^2}{b} I_3(\psi_0)\right] + 2hHn_w E_s \tag{13}$$

Simplification of Eq. (13) in order to calculate P gives:

$$P = \frac{1}{2H - b} \times \left\{ n_A M_0 \left[32\frac{Hb}{h} I_1(\psi_0) + 4\sqrt{3}S\bar{\alpha} + 8\frac{H^2}{b} I_3(\psi_0)\right] + 2hHn_w E_s \right\} \tag{14}$$

The least possible value of the mean crushing force, P, can be obtained from minimizing Eq. (14) with respect to two unknown parameters, the half-wavelength of the folding mode, H, and the small radius of the toroidal shell, b. So:

$$\frac{\partial P}{\partial H} = 0, \frac{\partial P}{\partial b} = 0 \tag{15}$$

4- Calculation of n_A and n_w

The number of the crushed folding elements, n_A, can be obtained by division of the folded area to the basic folding element area. The basic folding element area, shown in Fig. 12 is $\sqrt{3}/4\, S^2$. Although the folded zone is a skew polygon, the folded area can be estimated as $\pi/4\, \bar{d}^2$, where $\bar{d}$ can be written as:

$$\bar{d} = d + k'S \tag{16}$$

in which d and S are the diameter of the projectile and the cell size, respectively, and k' is a constant coefficient.

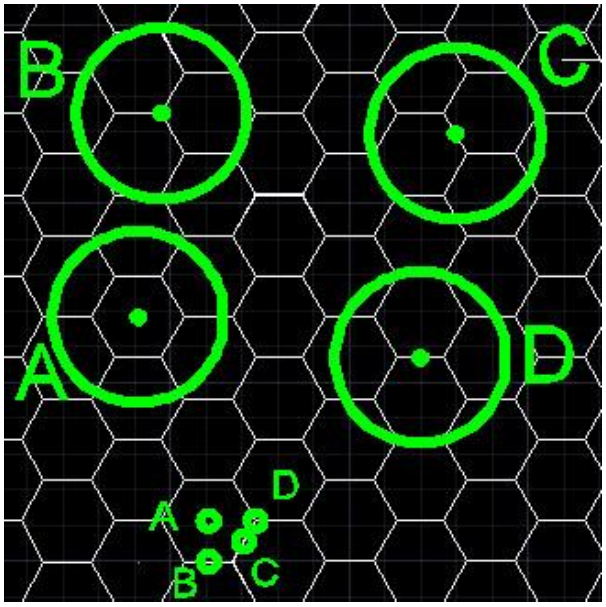

Fig. 14. Four different cases of the projectile's position

Therefore, n_A can be determined as:

$$n_A = \pi / \sqrt{3} \left(\frac{d + k'S}{S} \right)^2 \quad (17)$$

On the other hand, the number of the sheared walls, n_w, is written in Eq. (18) where k is another constant coefficient.

$$n_w = k \frac{d}{S} \quad (18)$$

In order to determine constant coefficients, k and k', four different cases A, B, C, and D, shown in Fig. 14, such as the position of projectile center on the honeycomb, are considered. In case A, the projectile and a cell are concentric. In case B, the projectile center is located on one of the hexagonal corners. Finally, in cases C and D projectile center is located in the middle of a single and dual wall, respectively.

A skew polygon is obtained by connecting the cutting off positions. Table 2 illustrates the values of constant coefficients k and k' for different values of projectile diameter and cell size. Average values of k and k' are 4.73 and 0.63, respectively.

5- Results and Discussion

Results of the experiments including the absorbed energy, specific energy, displacement of densification, slope of the elastic region, peak load value, and displacement corresponding to peak load have been shown in Table 3. In this article, specific energy is defined as the absorbed energy per unit specimen height. In addition, densification strain and strain at peak load are defined as the displacement values corresponding respectively to the densification and peak load per initial height of the sample. Since the loading speed of samples, SM11 and SM12, is relatively high, the test could not be performed completely and unfortunately, the absorbed energy and other data cannot be obtained perfectly.

Comparison between SM3 and SM1 and also SM5 and SM2 shows that however the densification strain of a honeycomb under local loading, for both flat and spherical projectiles, is e few more than densification strain under global loading, the metal honeycomb, subjected to a quasi-static loading by a flat projectile, absorbs energy at least 60% more than the global loading condition. On the other hand, although the maximum load of local loading is more than that of the global loading, but the maximum force of the local loading occurs at the relatively high strains.

Comparison SM3 and SM4 and also SM5 and SM6 illustrate that the absorbed energy is not completely related to the square of the projectile diameter. Furthermore, it seems that the densification strain increases by increasing the projectile diameter.

It can be seen from SM4 and SM7 and also SM 6 and SM8 that however, the densification of the spherical projectile loading occurs at higher strain, but the absorbed energy and maximum load of a honeycomb under spherical projectile loading is significantly less than those of the flat projectile loading.

Since the heights of specimens SM9 and SM10 are less than specimens SM4 and SM7, for better comparison, it is useful to

Table 2. Values of k and k' for different values of projectile's diameter and cell size

No.	d/S Ratio	Projectile's Position	k	k'
1	3.1	A	5.19	0.99
2	3.1	B	5.84	0.85
3	3.1	C	4.55	0.30
4	3.1	D	3.08	0.30
5	4.6	A	5.19	0.63
6	4.6	B	4.33	0.33
7	4.6	C	4.76	0.67
8	4.6	D	4.33	0.67
9	6.2	A	5.19	1.12
10	6.2	B	4.55	0.69
11	6.2	C	5.36	0.62
12	6.2	D	4.55	0.62
13	8.9	A	4.18	0.36
14	8.9	B	4.86	0.43
15	8.9	C	4.63	0.73
16	8.9	D	4.63	0.73
17	11.6	A	4.85	0.88
18	11.6	B	4.59	0.49
19	11.6	C	4.68	0.62
20	11.6	D	4.50	0.62

Table 3. Experimental results of specimens SM1 to SM10

Sample Index	Absorbed Energy (J)	Specific Energy (J/m)	Densification Strain (%)	Maximum Load (N)	Strain at peak (%)
SM1	9.06	453	74.50	809.26	4.00
SM2	7.38	410	68.33	754.88	4.94
SM3	14.78	739	82.50	991.42	77.50
SM4	4.10	205	80.00	312.88	71.00
SM5	13.73	763	72.22	1321.06	76.39
SM6	3.42	190	71.11	347.65	52.83
SM7	2.03	102	82.50	157.22	31.95
SM8	0.87	48	82.78	89.86	45.44
SM9	2.70	213	86.61	307.64	71.73
SM10	1.07	84.3	94.45	171.96	49.06

compare the specific energy instead of absorbed energy. It seems that in the flat projectile loading the specific energy decreases by increasing the specimen height, while in the spherical projectile loading, specific energy increases by increasing the specimen height. On the other hand, for both flat and spherical projectiles, densification strain decreases by increasing the specimen height.

Mean crushing load can be calculated by dividing the absorbed energy by the displacement of densification. Table 4 compares the experimental and analytical results for local mean crushing loads of samples SM3, SM4, SM5, and SM6. All samples are constructed from AL 3003-H18. Results show that the presented theoretical model predicts the mean crushing load of the metal hexagonal honeycomb under flat projectile compression with a 9.3% error. Table 2 illustrated that in the small values of d/S ratios, constant coefficients k and k' depend on the position of the projectile center on the honeycomb plane. Therefore, the difference between the theoretical and experimental values of SM6 can be in the results of the very

Table 4. Comparison between the experimental and theoretical values of mean crushing load

Sample Index	Experimental (N)	Analytical (N)	Error (%)
SM3	896	959	7.14
SM4	256	270	5.47
SM5	1056	989	6.34
SM6	263	311	18.25

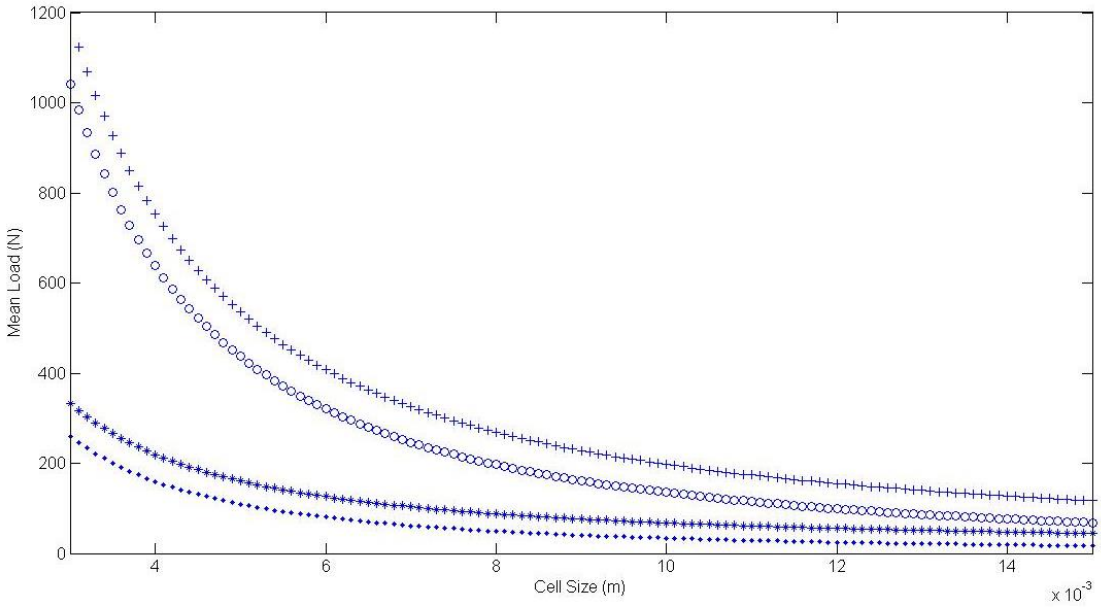

Fig. 15. Variation of theoretical mean crushing load in terms of cell size (Local d=32mm +, Global d=32mm o, Local d=16mm *, Global d=16 mm .)

small d/S ratio.

Figs. 15 and 16 show the mean crushing load, required for the folding of metal hexagonal honeycomb under quasi-static flat projectile punch, in terms of cell size and wall thickness, respectively. For better comparison, the mean crushing force in the global loading is also shown. The mean crushing load decreases by increasing the value of cell size, while it increases by increasing the value of wall thickness. Furthermore, curves illustrate that the difference between the local and global loads is increased by increasing the wall thickness, while it is decreased by increasing the cell size.

Fig. 17 shows the variations of the mean crushing load of a honeycomb specimen, loaded by a flat projectile, in terms of projectile diameter. It can be shown that, in the global loading, the mean crushing load is a function of d^2, in which d is the specimen diameter.

6- Conclusion

In this article, the behavior of metal hexagonal honeycomb under quasi-static out of plane punch loading was investigated, experimentally and analytically. Experimental results show that the absorbed energy is not only a function of the geometrical dimensions of honeycomb cells such as the cell size and wall thickness, but it is also related to the projectile shape and diameter, honeycomb height, and loading speed. Absorbed energy increases by increasing the honeycomb wall thickness, projectile diameter, and loading speed, while it decreases by increasing honeycomb cell size and height.

The perforated zone of the honeycomb samples under local out of plane loading are not perfectly circulars, but they are similar to skew polygons or elliptic, are extended in direction of the dual walls. It leads to the mean crushing force of the aluminum honeycomb sample under local loading be significantly greater than its global loading.

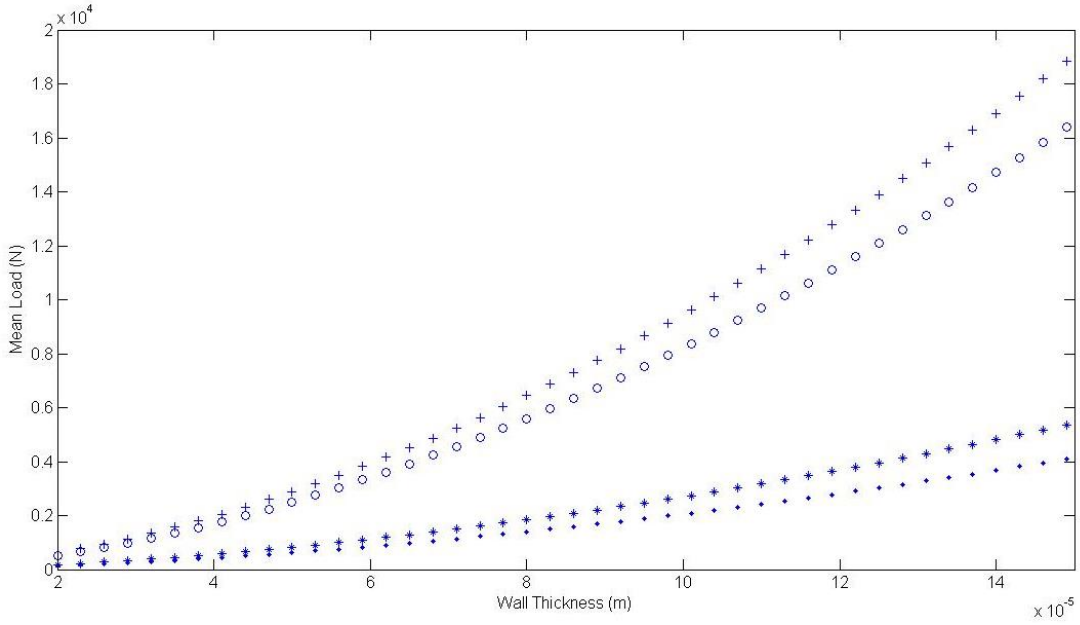

Fig. 16. Variation of theoretical mean crushing load in terms of wall thickness (Local d=32mm +, Global d=32mm o, Local d=16mm *, Global d=16 mm .)

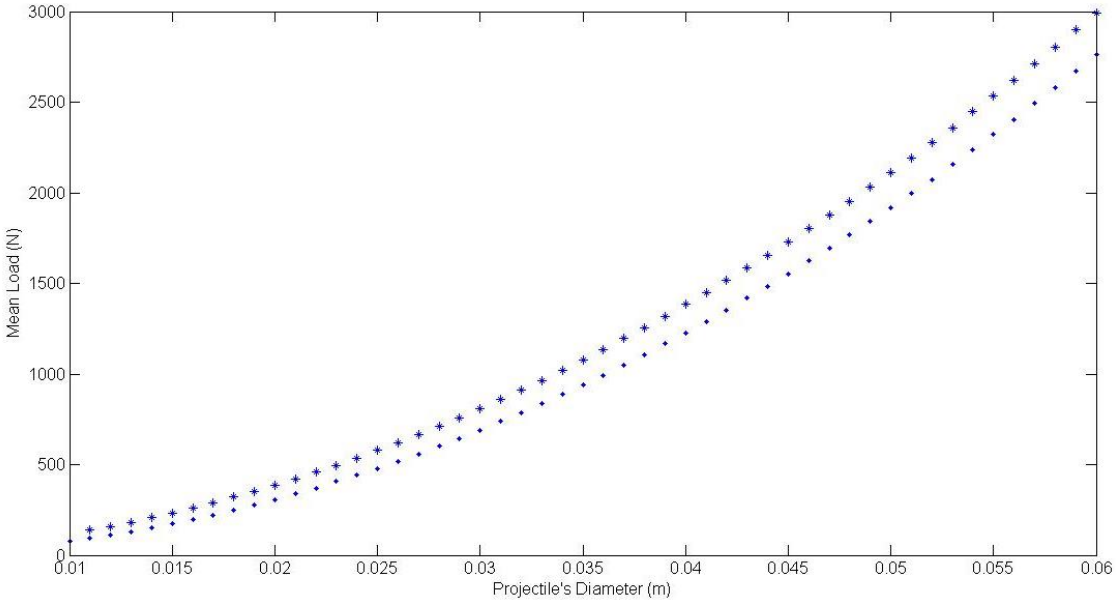

Fig. 17. Variation of theoretical mean crushing load in terms of projectile diameter (Local loading *, Global loading .)

In the analytical section, the mean crushing load of metal hexagonal honeycomb subjected to the penetration of flat nose projectile has been calculated by considering the skew polygon surface and the dissipated energy term in cutting-off of the honeycomb walls. Results show that the local mean crushing load is greater than that of the global one and the difference between these two values increases by increasing the honeycomb wall thickness and projectile diameter and decreasing the honeycomb cell size.

7- Declarations

7- 1- Availability of data and materials

However the presented theory has been verified based on the experiments, it can be shown that the mentioned theory could be simplified for the quasi-static global crushing loading of the hexagonal honeycomb, which is found in [22]

7- 2- Competing interests

The authors declare that they have no competing interests.

8.3 Funding

Not applicable

8.4 Authors' contributions

M-ZM has made substantial contributions to the conception and design, performing the experiments, acquisition of data, proposing the mathematical modeling, analysis and interpretation of data and wrote the manuscript. M-S has made substantial contributions to the conception and design, analysis and interpretation of data and revising the manuscript.

8.5 Acknowledgements

Supported by the strengths of material and the impact mechanics libraries of the Amirkabir University of Technology.

8.6 Authors' information

M. Zarei Mahmoudabadi, born in 1985, is currently a Ph.D. Student at the department of mechanical engineering, Amirkabir University of Technology, Iran.

M. Sadighi, born in 1960, is currently the professor at the department of mechanical engineering, Amirkabir University of Technology, Iran. His research interests include mechanics of composite sandwich materials, energy absorbers and behavior of the fiber metal laminates.

References

[1] W. Goldsmith, J.L. Sackman, An experimental study of energy absorption in impact on sandwich plates, International Journal of Impact Engineering, 12(2) (1992) 241-262.

[2] E. Wu, W.-S. Jiang, Axial crush of metallic honeycombs, International Journal of Impact Engineering, 19(5-6) (1997) 439-456.

[3] G. Liaghat, A. Alavinia, A comment on the axial crush of metallic honeycombs by Wu and Jiang, International Journal of Impact Engineering, 28(10) (2003) 1143-1146.

[4] J. Klintworth, W. Stronge, Plane punch indentation of a ductile honeycomb, International journal of mechanical sciences, 31(5) (1989) 359-378.

[5] S.A. Galehdari, M. Kadkhodayan, S. Hadidi-Moud, Low velocity impact and quasi-static in-plane loading on a graded honeycomb structure; experimental, analytical and numerical study, Aerospace Science and Technology, 47 (2015) 425-433.

[6] W. Goldsmith, D.L. Louie, Axial perforation of aluminum honeycombs by projectiles, International Journal of Solids and Structures, 32(8-9) (1995) 1017-1046.

[7] F. Cote, V. Deshpande, N. Fleck, A. Evans, The out-of-plane compressive behavior of metallic honeycombs, Materials Science and Engineering: A, 380(1-2) (2004) 272-280.

[8] S. Heimbs, P. Middendorf, M. Maier, Honeycomb sandwich material modeling for dynamic simulations of aircraft interior components, in: 9th international LS-DYNA users conference, 2006, pp. 1-13.

[9] A.A. Nia, S. Razavi, G. Majzoobi, Ballistic limit determination of aluminum honeycombs—experimental study, Materials Science and Engineering: A, 488(1-2) (2008) 273-280.

[10] T. Asada, Y. Tanaka, N. Ohno, Two-scale and full-scale analyses of elastoplastic honeycomb blocks subjected to flat-punch indentation, International Journal of Solids and Structures, 46(7-8) (2009) 1755-1763.

[11] M. Khoshravan, M.N. Pour, Numerical and experimental analyses of the effect of different geometrical modelings on predicting compressive strength of honeycomb core, Thin-Walled Structures, 84 (2014) 423-431.

[12] Z. Wei, V. Deshpande, A. Evans, K. Dharmasena, D. Queheillalt, H. Wadley, Y. Murty, R. Elzey, P. Dudt, Y. Chen, The resistance of metallic plates to localized impulse, Journal of the Mechanics and Physics of Solids, 56(5) (2008) 2074-2091.

[13] G. Petrone, S. Rao, S. De Rosa, B. Mace, F. Franco, D. Bhattacharyya, Behaviour of fibre-reinforced honeycomb core under low velocity impact loading, Composite Structures, 100 (2013) 356-362.

[14] A.P. Meran, T. Toprak, A. Muğan, Numerical and experimental study of crashworthiness parameters of honeycomb structures, Thin-Walled Structures, 78 (2014) 87-94.

[15] M.Z. Mahmoudabadi, M. Sadighi, Experimental investigation on the energy absorption characteristics of honeycomb sandwich panels under quasi-static punch loading, Aerospace Science and Technology, 88 (2019) 273-286.

[16] S. Wang, H. Wang, Y. Ding, F. Yu, Crushing behavior and deformation mechanism of randomly honeycomb cylindrical shell structure, Thin-Walled Structures, 151 (2020) 106739.

[17] T. Wierzbicki, Crushing analysis of metal honeycombs, International Journal of Impact Engineering, 1(2) (1983) 157-174.

[18] W. Abramowicz, T. Wierzbicki, Axial crushing of multicorner sheet metal columns, (1989).

[19]] M.Z. Mahmoudabadi, M. Sadighi, A study on metal hexagonal honeycomb crushing under quasi-static

loading, World Academy of Science, Engineering and Technology (53), (2009) 677-681.

[20] M.Z. Mahmoudabadi, M. Sadighi, A theoretical and experimental study on metal hexagonal honeycomb crushing under quasi-static and low velocity impact loading, Materials Science and Engineering: A, 528(15) (2011) 4958-4966.

[21] Z. Li, T. Wang, Y. Jiang, L. Wang, D. Liu, Design-oriented crushing analysis of hexagonal honeycomb core under in-plane compression, Composite Structures, 187 (2018) 429-438.

[22] M.Z. Mahmoudabadi, M. Sadighi, A study on the static and dynamic loading of the foam filled metal hexagonal honeycomb–Theoretical and experimental, Materials Science and Engineering: A, 530 (2011) 333-343.

HOW TO CITE THIS ARTICLE

M. Zarei Mahmoudabadi, M. Sadighi, Out of Plane Punch of Aluminum Hexagonal Honeycomb Using Flat Nose and Spherical Projectiles, AUT J. Mech Eng., 5(4) (2021) 553-570.

DOI: 10.22060/ajme.2021.18838.5924